A Journal of the Gesellschaft Deutscher Chemiker

Angewandte International Edition Chemie

GDCh

www.angewandte.org

Accepted Article

Title: Dynamic Stereoselection of Peptide Helicates and Their Selective Labeling of DNA Replication Foci in Cells

Authors: Jacobo Gómez-González, Yolanda Pérez, Giuseppe Sciortino, Lorena Roldan-Martín, José Martínez-Costas, Jean Didier Maréchal, Ignacio Alfonso, Miguel Vázquez, and M. Eugenio Vazquez

To be cited as: *Angew. Chem. Int. Ed.* 10.1002/anie.202013039

Link to VoR: https://doi.org/10.1002/anie.202013039

WILEY-VCH

10.1002/anie.202013039

WILEY-VCH

RESEARCH ARTICLE

Dynamic Stereoselection of Peptide Helicates and Their Selective Labeling of DNA Replication Foci in Cells

Jacobo Gómez-González,[a] Yolanda Pérez,[b],§ Giuseppe Sciortino,[c,d],§ Lorena Roldan-Martín,[c] José Martínez-Costas,[e] Jean-Didier Maréchal,[c] Ignacio Alfonso,[f] Miguel Vázquez López,*,[g] M. Eugenio Vázquez*,[a]

Dedicated to baby Vega

Abstract: Although largely overlooked in peptide engineering, coordination chemistry offers a new set of interactions that opens unexplored design opportunities for developing complex molecular structures. In this context, we report new artificial peptide ligands that fold into chiral helicates in the presence of labile metal ions such as Fe(II) and Co(II). Heterochiral β-turn promoting sequences encode the stereoselective folding of the peptide ligands and define the physicochemical properties of their corresponding metal complexes. CD and NMR spectroscopy in combination with computational methods allowed us to identify and determine the structure of two isochiral ΛΛ-helicates, folded as topological isomers. Finally, in addition to the in vitro characterization of their selective binding to DNA three-way junctions, cell microscopy experiments demonstrated that a rhodamine-labeled Fe(II) helicate was internalized and selectively stains DNA replication factories in functional cells.

[a] Dr. J. Gómez-González., A. Prof. M. E. Vázquez*
Centro Singular de Investigación en Química Biolóxica e Materiais Moleculares (CiQUS), Departamento de Química Orgánica, Universidade de Santiago de Compostela, Spain.
E-mail: *eugenio.vazquez@usc.es*

[b] Dr. Y. Pérez
NMR Facility, Institute of Advanced Chemistry of Catalonia (IQAC-CSIC), Jordi Girona 18-26, 08034 Barcelona, Spain.

[c] L. Roldán-Martín, Dr. G. Sciortino, Prof. J.-D. Maréchal
Departament de Química, Universitat Autònoma de Barcelona, 08193 Cerdanyola, Spain

[d] Dr. G. Sciortino
Institute of Chemical Research of Catalonia (ICIQ)
Avgda. Països Catalans, 16, 43007 Tarragona, Spain.

[e] Prof. J. Martínez-Costas
Centro Singular de Investigación en Química Biolóxica e Materiais Moleculares (CiQUS), Departamento de Bioquímica y Biología Molecular, Universidade de Santiago de Compostela, Spain.

[f] Dr. I. Alfonso
Department of Biological Chemistry, Institute of Advanced Chemistry of Catalonia (IQAC-CSIC), Jordi Girona 18-26, 08034 Barcelona, Spain

[g] Prof. M. Vázquez López*
Centro Singular de Investigación en Química Biolóxica e Materiais Moleculares (CiQUS), Departamento de Química Inorgánica, Universidade de Santiago de Compostela, Spain.
E-mail: *miguel.vazquez.lopez@usc.es*

§ These authors contributed equally to this work.

Supporting information for this article is given via a link at the end of the document.

Introduction

Metal ions offer vast opportunities for the structural control at the molecular scale; exploiting their different coordinative properties, researchers can create complex assemblies of great beauty and unique properties,[1] on par with the extraordinary structural and functional complexity displayed by peptides.[2] Bridging the architectural potential of coordination chemistry with the structural predictability of peptide scaffolds would allow greater complexity in (supra)molecular designs by combining well-established peptide engineering concepts and tools with the supramolecular organization mediated by metal ions.[3]

Helicates are discrete metal complexes in which one or more organic ligands coil around—and coordinate—two or more metal ions.[4] Helicates display helical chirality, according to the orientation in which the ligands twist around the axis defined by the metal centers. Besides their fundamental interest in supramolecular chemistry,[5] helicates have also shown exciting properties as antifreeze agents,[6] as inhibitors of amyloid aggregation,[7] as well as G-quadruplex and three-way DNA binding properties that result in promising antimicrobial and antitumoral activities.[8] Therefore, as a challenging and relevant model system to demonstrate the potential of peptide platforms for engineering metallo-supramolecular entities, we decided to approach the stereoselective synthesis of peptide helicates.

We have previously described the synthesis of peptide ligands containing a O1Pen-2,2'-bipyridine amino acid derivative, which predictably fold into coordination compounds with defined chirality,[9] including self-assembled helicates,[10] in the presence of metal ions. Unfortunately, the two hydrophobic Pro-Gly β-turns that encoded the folding of these peptide ligands,[11] also made our designs poorly soluble and prone to aggregation. Moreover, these helicates, based on the kinetically labile Fe(II)-trisbipyridine coordination, were inherently dynamic and displayed relatively weak metal binding constants. Herein we describe the rational design of alternative oligocationic peptide helicates with improved solubility and thermodynamic stability, and the synthesis of kinetically inert Co(III) helicates through oxidation of their dynamically assembled Co(II) precursors. We also show that these optimized self-assembled Fe(II) helicates bind to three-way DNA junctions *in vitro* and in functional cells, selectively labelling DNA replication foci in the cell nuclei.

10.1002/anie.202013039

WILEY-VCH

RESEARCH ARTICLE

Results and Discussion

Rationale

In order to improve the solubility of the peptide ligands (and that of the final helicates) we decided to replace the original β-turn modules, (D/L)-Pro-Gly, with more polar sequences that were also capable of inducing a reverse β-turn to direct the folding of the peptide chain into the desired three-stranded helicates.[12] Based on the known tendency of heterochiral sequences to promote the formation of type *II* or type *II′* β-turns,[13] we focused our attention on the combination of residues with mixed chirality, D-D-L (or its mirror image L-L-D) which were reported to increase turn formation and stability in short peptides.[14] This pattern was very attractive for our purposes, because it allowed us great freedom in the choice of the residues in the loops, as long as they maintained their relative chirality. Thus, in order to maximize the solubility, and considering the prevalence of Arg residues in protein-DNA complexes,[15] as well as the known beneficial effects of arginine residues in DNA-binding helicates,[16] we selected the sequences L-Arg–L-Pro–D-Arg and D-Arg–D-Pro–L-Arg to define the β-turns and direct the folding of the peptide ligands into two enantiomeric peptide helicates, **LLD** and **DDL** respectively (Scheme 1). Additionally, we replaced the original O1PenBpy building block with a shorter β-Ala derivative (βAlaBpy) to reduce the conformational freedom of the loops and therefore increase the preorganization and thermodynamic stability of the assembled helicates.

Synthesis and characterization of the peptide helicates

The precursor peptide ligands **LLD** and **DDL** were obtained by standard Fmoc solid-phase peptide synthesis protocols.[17] The Bpy ligands were introduced in the form of an Fmoc-protected building block, Fmoc-βAlaBpy-OH (**1**, Scheme 1), which was synthesized with minor modifications of reported procedures reported for the synthesis of Fmoc-O1PenBpy-OH.[9] The final peptide ligands were purified by HPLC, and their identity confirmed by mass spectrometry (See the Experimental Section and Supporting Information for details). As expected, the four charged arginine residues in the sequence made these new peptide ligands readily soluble in water, thus radically improving the poor solubility of our previous design.[10]

The assembly of the Fe(II)$_2$**LLD** and Co(II)$_2$**LLD** helicates in solution was characterized by monitoring the quenching in the fluorescence emission intensity of the 5'-amido-[2,2'-bipyridine]-5-carboxamide upon metal coordination (Figure 1a).[18,19] The resulting titration profile was successfully fitted to a 1:2 binding mode with dissociation constants of about 0.5 and 0.4 μM for the first, and second metal ion coordination for both Fe(II) and Co(II).[20] These values are two orders of magnitude smaller than those of the original O1Pen-based peptide helicates,[10] demonstrating the beneficial effect of the reduced conformational freedom of the βAlaBpy building block leading to helicates high thermodynamic stability. Furthermore, the observed positive cooperativity suggests that the coordination of the first metal ion further preorganizes the peptide for the binding of the second ion.[21] MALDI spectra of the solutions at saturating concentrations of metal ions showed peaks at 2555.06 and 2561.02, consistent with the formation of the Fe(II)$_2$**LLD** and Co(II)$_2$**LLD** helicates, respectively (See Figure S5 and S7 in the Supporting information). As expected, the fluorescence titrations with the **DDL** ligand reproduced these results.

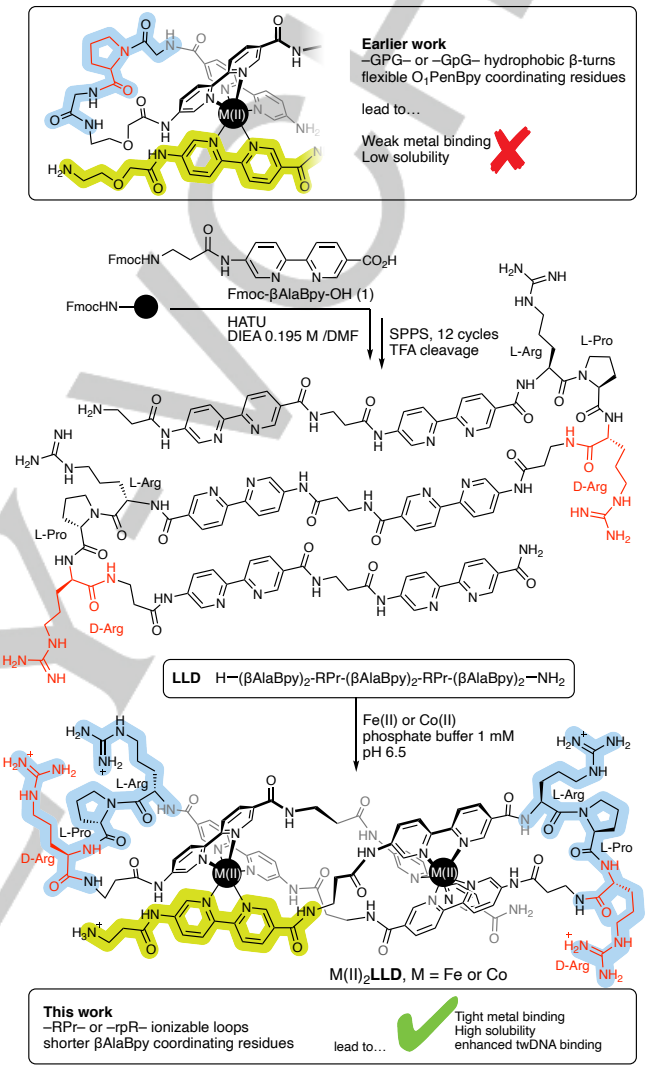

Scheme 1. Top: Key elements in our first-generation design using (D/L)-Pro-Gly and flexible O1PenBpy building block. Bottom: Solid-phase peptide synthesis of the helicate ligand **LLD** using the Fmoc-βAlaBpy-OH building block. β-turn sequences (RPr) are highlighted in light blue, and one βAlaBpy building block in green. After cleavage and purification, the helicate is stereoselectively folded under thermodynamic control in the presence of coordinating metal ions, Fe(II) or Co(II). The **LLD** ligand contains two loops featuring the heterochiral L-Arg–L-Pro–D-Arg sequence, while the **DDL** contains enantiomeric D-Arg–D-Pro–L-Arg loops (H-(βAlaBpy)$_2$-rpR-(βAlaBpy)$_2$-rpR-(βAlaBpy)$_2$-NH$_2$). L-amino acids are indicated in upper-case, and D-amino acids in lower case (i.e., R, P for L-Arg and L-Pro, and r, p for D-Arg and D-Pro).

Importantly, the **LLD** and **DDL** peptide ligands displayed mirror image circular dichroism spectra. The CD was dominated by a strong Cotton effect band at c.a. 320 nm, which pointed to a significant preorganization of the peptide chain and the effective chiral induction by the heterochiral β-turn modules in combination

10.1002/anie.202013039

with π-stacking interactions between the bipyridine units.[9a, 22] Addition of Fe(II) ions to a **LLD** solution resulted in a large enhancement of the positive Cotton effect band at c.a. 320 nm, as well as the appearance of a weaker negative Cotton effect band about 525 nm, both bands consistent with the formation of a ΛΛ- (or *M*) helicate (Figure 1b). Likewise, the enantiomeric peptide ligand **DDL** gave rise to opposite bands at 320 and 525 nm, as expected for the induction of the mirror image ΔΔ- (or *P*) helicate (Figure 1b). Taken together, these data are consistent with a dynamic process in which the mixture of the peptide ligands and the Fe(II) ions evolves towards the more stable folded helicates under thermodynamic control.

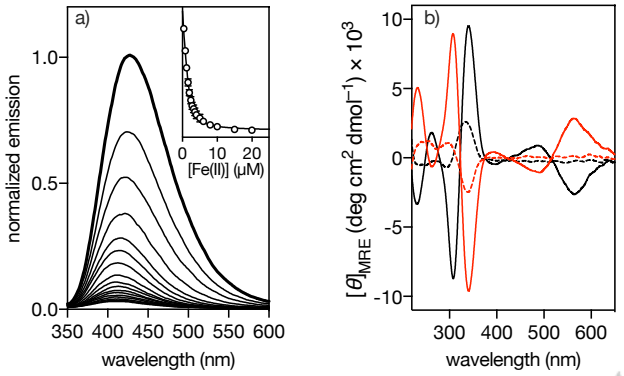

Figure 1. Titration of the **LLD** peptide ligand with Fe(II) ions. a) Normalized emission spectrum of a 2 μM solution of **LLD** in 1 mM phosphate buffer NaCl 10 mM, pH 6.5 (thick line), and spectra of the same solution in the presence of increasing concentrations of Fe(II) ions (thin lines); inset showing the titration profile of three independent experiments and best fit to a one to two binding model (same range as main plot); b) circular dichroism spectra of 5 μM solutions of **LLD** (black dashed line) and **DDL** (red dashed line) in 1 mM phosphate buffer NaCl 10 mM, pH 6.5, and in the presence of 25 μM Fe(II) ions (same colors, continuous lines).

Locking the dynamic equilibrium by oxidizing Co(II) to Co(III)

The dynamic self-assembly of the helicates limits their potential applications and prevents their detailed structural characterization, because these self-assembled species are intrinsically dynamic and could disassemble, exchange ligands, or modify their structure or association state in response to changes in their environment.[23] To overcome these limitations we tested the *in situ* formation of robust Co(III) helicates by oxidation of the dynamically assembled Co(II) analogs.[24] This strategy has been extensively used for the assembly of kinetically-inert metal complexes and described for the immobilization of His-tagged proteins ,[25] but, to our knowledge, has never been used in the case of artificial metallopeptides. Thus, preformed solution of the Co(II)$_2$**LLD** helicate was treated with ceric ammonium nitrate, $(NH_4)_2Ce(NO_3)_6$, and analyzed by HPLC. Gratifyingly, while the labile helicates Fe(II)$_2$**LLD** and Co(II)$_2$**LLD** could never be observed in the acidic RP-HPLC conditions (0.1% TFA H_2O/CH_3CN), after oxidation we could isolate a new peak with mass consistent with the formation of the Co(III)$_2$**LLD** helicate, and a circular dichroism spectrum indicating the presence of species with the expected ΛΛ-chirality (Figure S10).[26]

Structural determination of two helicate topoisomers

The kinetic stability of this new Co(III)$_2$**LLD** helicate allowed us to obtain 2D NMR spectra with higher quality than those with the complex with Fe(II), and the 1D ^{1}H NMR spectra confirmed the folding of the peptide ligand into stable and ordered structures (Figure S13, Supporting Information), which encouraged us to pursue their detailed structural characterization in solution. Based on our previous work with metallopeptides and NMR studies of dinuclear ruthenium (II) polypyridyl complex,[27] we decided to apply the standard approach for peptide sequence assignment and structural characterization,[28] which consists in 2D NMR data acquisition in protonated solvent (90% H_2O/10% D_2O), proton/carbon resonance assignment and the use of the identified NOEs from the amino acid/βAla residues to obtain distance restraints for molecular dynamics (See the Supporting Information for a more detailed description of this strategy, 1D/2D spectra and NOEs restraints). Curiously, the isolated fraction (Supporting Information, Figure S8) showed two main components in solution, isomers, **A** and **B**, in slow exchange in the NMR chemical shift timescale (Figure 2). The resonances corresponding to 1D aromatic/amide region and 2D ^{1}H-^{1}H NOESY correlations for N*H*-α/βC*H*$_2$ (in particular, for β-Ala3/5 at helicate turns) revealed the conformational flexibility of the peptidic turns in the metal complex. In contrast, the region of the Bpy ligands coordinated to the metal ions is more rigid. For this reason, due to ^{15}N T1 long relaxation times, the ^{15}N bipyridine resonances could not be observed in the ^{15}N-^{1}H HMBC spectrum (data not shown). Based on the NMR experimental data,[29] and considering the similar coordination geometries of the Co(III) and Fe(II) trisbipyridyl complexes, we generated two reasonable starting point models of the Fe(II) isomers **A** and **B**, and assessed their stability by Molecular Dynamics (MD) simulations in explicit solvent and periodic boundary conditions (See the Supporting Information for details). During the simulations, the helical twist of the helicates, as well as the octahedral coordination geometry of the Fe(II) metal centers with the Bpy units were conserved. The root-mean square deviation (RMSD) on the heavy atoms (excluding the side chains) was computed during the trajectories using the minimized initial structures as a reference. In both cases the trajectories stabilize after the first 25 ns, reaching relatively stable RMSDs of 1.5 and 2.5 Å in average for isomers **A** and **B**, respectively. A cluster analysis performed on the full-length MDs showed a predominant geometry occupied about 64% and 89% of the total conformation repartition for **A** and **B**. Starting from the representative structures of these clusters, further molecular dynamics refinements where carried out along 60 additional ns under NOE's distance restraints (Tables S3 and S4) in explicit solvent. The NMR refinement was performed using SANDER including flat-bottom NOE-derived distance potential function.[30] Overall, the results show that the two model structures, **A** and **B**, are valid candidates consistent with the experimental observations (see Experimental Section for a detailed analysis). Helicates **A** and **B** are topoisomers, that is, they have the same chirality but different connectivity between the Bpy units around the metal centers. In isomer **A**, the N-terminal (blue, Figure 2) and the C-terminal (red, Figure 2) bipyridine units are placed in the same side of the metallocylinder, whereas in isomer **B**, both terminal Bpy units are disposed in opposite sides of the helicate.[31]

10.1002/anie.202013039

WILEY-VCH

RESEARCH ARTICLE

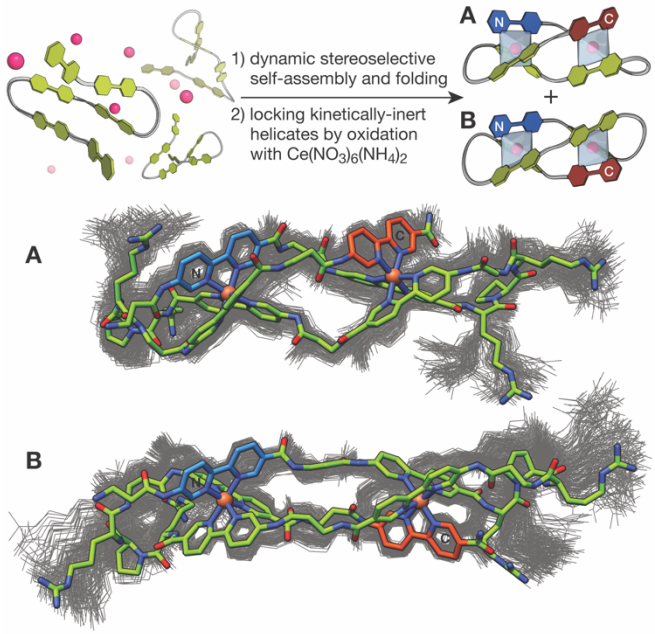

Figure 2. Top: assembly-followed-by-fixing approach for the construction of kinetically-inert Co(III)$_2$**LLD** peptide helicates. The initial dynamic selection under thermodynamic control is followed by the oxidation of Co(II) to Co(III) to yield kinetically-inert complexes **A** and **B**, which have the same chirality, but different topology. Bottom: representative structures for the Fe(II) helicates of the two most populated clusters of the MD trajectories (stick) together with 100 frames of each trajectory. N-terminal bipyridine in blue, and C-terminal bipyridine in red.

The peptide helicates selectively recognize three-way DNA junctions in vitro

Helicates are known to selectively interact with DNA three-way junctions by insertion into the hydrophobic cavity created by the surface of the base pairs at the center of the DNA junction.[8d,32] To study the DNA binding properties of these new peptide helicates we prepared a 2 μM solution of a fluorescein-labeled three-way junction DNA (**Flu-twDNA**), and measured its luminescence after the addition of successive aliquots of a solution of the preformed helicate Fe(II)$_2$**LLD**. The progressive quenching of the fluorescein emission at 515 nm could be fitted to a simple 1:1 binding mode (**Flu-twDNA**/Fe(II)$_2$**LLD**) with an apparent dissociation constant K_D ≈ 0.45 μM,[33] which is in line with the data obtained for the original Pro-Gly Fe(II) peptide helicate (Figure 3). Curiously, in the case of the helicate Co(III)$_2$**LLD**, the titration profile of the emission intensity at 515 nm had to be fitted to a more complex model with a lower-affinity binding site, likely corresponding to the insertion of the Co(III)$_2$**LLD** metallopeptide in the hydrophobic cavity, with a K_D ≈ 7.9 μM, and three equivalent higher-affinity sites (K_D ≈ 4.9 μM), which based on reported X-ray structures of related helicate/DNA complexes could correspond to nonspecific stacking interactions of the helicate with the blunt ends of the twDNA arms.[8d]

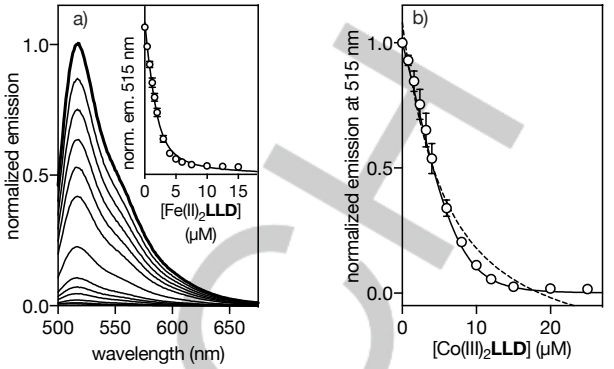

Figure 3. a) Normalized emission spectra of a titration of a 2 μM solution of the fluorescein-labeled three-way junction DNA, **Flu-twDNA**, in 1 mM phosphate buffer, 10 mM NaCl, pH 6.5 (thick line) with increasing concentrations of the Fe(II)$_2$**LLD** helicate (thin lines); inset: corresponding normalized titration profile of the fluorescein quenching at 515 nm and best fit to a one to one binding model; b) Normalized emission of a 2 μM solution of the fluorescein-labeled three-way junction DNA, **Flu-twDNA**, in 10 mM phosphate buffer, 100 mM NaCl, 10 mM $MgCl_2$, pH 6.5 with increasing concentrations of the Co(III)$_2$**LLD**; the best fit to a simple one to one binding model is shown as a dashed line, and the fit to a model including non-specific binding is shown as a continuous line. Titration data are the average of three independent experiments. **Flu-twDNA**, **Y1** Flu-5'–TTTT CAC CGC TCT GGT CCT C–3'; **Y2** 5'–CAG GCT GTG AGC GGT G–3'; **Y3** 5'–GAG GAC CAA CAG CCT G–3'.

To better understand the interaction of the Fe(II) and Co(III) helicates with the DNA, we carried out electrophoretic mobility shift assays (EMSA) in polyacrylamide gel under non-denaturing conditions and using *SYBRGold* as the DNA stain.[34] In agreement with the fluorescence studies, we found that incubation of **twDNA** with increasing concentrations of the preformed Fe(II)$_2$**LLD** helicate resulted in the appearance of new slow-migrating band, consistent with the formation of the **twDNA**/Fe(II)$_2$**LLD** complex (Figure 4a). As expected for a high-affinity interaction, complete band shift is observed already at the lowest concentrations tested, and gives rise to a single new band with no smearing, even at high concentration of the Fe(II)$_2$**LLD** helicate. On the other hand, no new slow-migrating bands were observed upon incubation of Fe(II)$_2$**LLD** with a double-stranded DNA (**dsDNA**), which confirms the low affinity of this metallopeptide for regular B-DNA (Figure 4b). In agreement with the fluorescence titrations, the EMSA assays showed reduced affinity of the Co(III)$_2$**LLD** helicate for the **twDNA**, so that the saturation of the **twDNA** is only observed at the highest concentrations of Co(III)$_2$**LLD** (500 nM, Figure 4c). Remarkably, these assays also confirmed the tendency of the highly charged Co(III)$_2$**LLD** helicate to form non-specific complexes, as shown by the disappearance of the **dsDNA** band upon incubation with this helicate (Figure 4d).[35]

10.1002/anie.202013039

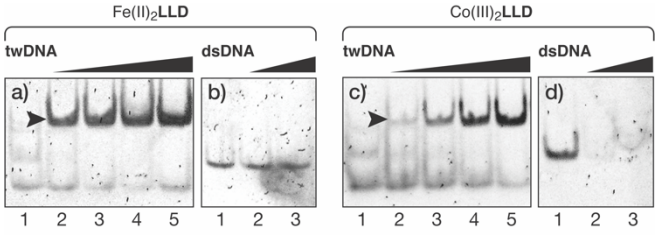

Figure 4. a) EMSA analysis of 200 nM **twDNA** in the presence of 0, 50, 100, 250, 500 nM of Fe(II)$_2$**LLD**. The new, slow-migrating band (indicated with an arrow), corresponds to the three-way DNA structure assembled in the presence of the Fe(II) helicate; b) 75 nM **dsDNA** with 0, 1000, and 1500 nM of Fe(II)$_2$**LLD**; gels in c) and d) correspond to the same concentrations of **twDNA** and **dsDNA** as a) and b) incubated with the same concentrations of the Co(III)$_2$**LLD** helicate (**dsDNA** 5'–AAC ACA TGC **AGG** ACG GCG CTT–3'; **twDNA, Y1** 5'–CAC CGC TCT GGT CCT C–3'; **Y2** 5'–CAG GCT GTG AGC GGT G–3'; **Y3** 5'–GAG GAC CAA CAG CCT G–3').

Based on the previous structural characterization, we used the new *GaudiMM* platform to obtain plausible models for two Fe(II)$_2$**LLD** topoisomers threaded into the DNA three-way junction.[36] The structures of the Fe(II) helicates extracted from the MD simulation under NOE constraints were docked to the DNA extracted from the X-ray structure of the helicate/three-way DNA junction complex reported by Hannon *et al*. (PDB ID: 2ET0).[8d] Energetically preferred orientations of the helicates inside the central cavity of the DNA three-way junction were found when considering displacements of up to 2.5 Angstroms along the ten lowest-energy normal mode vectors of the breathing modes of the twDNA (see Docking studies in the Experimental section), thus demonstrating that the accommodation of the helicates requires adaptation of the DNA target to the guests and that leads to a slightly different conformation than in the available X-ray structure taken as reference. Calculations with the two different isomers also showed a better accommodation of isomer **B** into the three-way DNA cavity showing higher scoring and lower clashes respect to the isomer **A** (see Supporting Information for further details). No clear penalizing interactions between the three-way DNA junction and the helicate units are observed although the center of mass of **B** aligned better with the **twDNA** and the entire complex fits more deeply into the DNA receptor. This is likely related to the smaller volume of **B** and its slightly more stretched geometry (Figure 5 and S17).

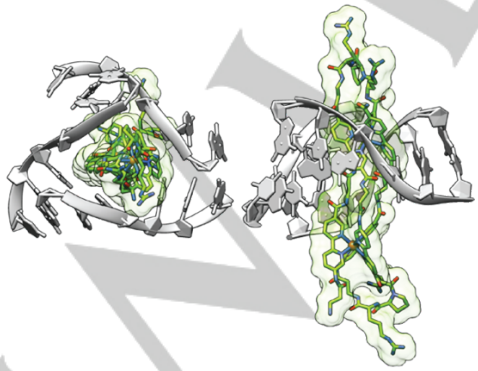

Figure 5. Lowest energy pose of isomer **B** of the Fe(II)$_2$**LLD** helicate in the central cavity of the **twDNA**. Left: top view showing the tight fit between the helicate and the **twDNA** hydrophobic site, which appears to be too narrow to comfortably accommodate isomer **A**. Right view of the same complex.

A rhodamine-labelled Fe(II)-helicate selectively labels DNA replication sites in functional cells

Having demonstrated the binding of these helicates to **twDNA** in vitro, we envisioned the application of these helicates to study these DNA structures in cells. Preliminary experiments in which the tetramethylrhodamine- and fluorescein-labeled Fe(II) helicates, Fe(II)$_2$**TAMRA-LLD** or Fe(II)$_2$**Flu-LLD**, [37] were incubated overnight with HeLa cells showed that these complexes remain trapped in endosomes (see Figure S28 in the Supporting information). [38] However, if the cells were pretreated with Digitonin,[39] then Fe(II)$_2$**TAMRA-LLD** was effectively internalized and showed in the red emission channel as a punctuated pattern in the cytoplasm and the nucleus (Figure 6a). Remarkably, the nuclear distribution of the helicate partially matched the localization of the DNA replication sites labeled with the proliferating cell nuclear antigen (PCNA) fused to GFP (Figure 6b), [40] which demonstrates that Fe(II) helicate is capable of targeting the three-way junctions transiently formed during DNA replication in functional cells (Figure 6c).[41] The staining of what appears to be the cell nucleolus is consistent with Fe(II)$_2$**TAMRA-LLD** binding to three-way RNA structures, which are also potential biological targets of helicates. [42] To our knowledge, this is the first demonstration *of in cellula* twDNA staining with designed fluorescent probes. As expected from the in vitro experiments, the Co(III)$_2$**TAMRA-LLD** helicate displayed poor specificity, leading to indiscriminate labeling in Digitonin treated cells (data not shown).

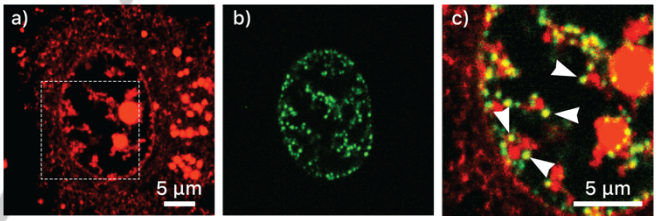

Figure 5. Fe(II)$_2$**TAMRA-LLD** selectively stains DNA replication sites. HeLa cells expressing protein GFP-PCNAL2 were incubated with 25 µg/ml Digitonin for 3 min, then 5 µM of **TAMRA-LLD** peptide ligand and 25 µM of $(NH_4)_2Fe(SO_4)_2$ for 30 min. a) Red channel emission showing the distribution of the rhodamine-labeled helicate; b) green channel, corresponding to the emission of the GFP-PCNAL2 probe labeling the DNA replication foci; c) overlay of the green and red channels of the square region shown in a) Arrows highlight some foci where the staining of GFP-PCNAL2 and Fe(II)$_2$**TAMRA-LLD** overlap.

Conclusion

We have demonstrated that peptide design rules can be applied to encode both structural and chiral information in *de novo* metallopeptides. In particular, we report new oligocationic peptides containing bipyridine ligands that fold into three-stranded helicates in the presence of Fe(II) ions and bind with high affinity and specificity to DNA three-way junctions. For the first time, we have determined the atomic structure of these peptide helicates by a combination of CD, NMR and sophisticated computational methods, and applied a new theoretical approach to explore the nature of their DNA complexes. Finally, we also demonstrate that the Fe(II)$_2$**TAMRA-LLD** helicate binds to DNA three-way junctions

in functional cells, selectively labeling DNA replication foci in the nuclei, thus demonstrating for the first time the selective staining of three-way DNA *in cellula* with designed fluorescent probes.

Acknowledgements

Financial support from the Spanish grant RTI2018-099877-B-I00, the *Xunta de Galicia* (grupos con potencial de crecemento ED431B 2018/04, Centro singular de investigación de Galicia accreditation 2016–2019, ED431G/09, and ED431B 2018/04) and the European Union (European Regional Development Fund - ERDF) are gratefully acknowledged. J. G.-G. thanks the Spanish *Ministry of Science and Innovation/Spanish Research Agency* for his FPI fellowship. We also wish to express our gratitude to Soraya Learte-Aymamí for her assistance in the optimization of the EMSA assays. I. A. thanks Spanish *Ministry of Science and Innovation/Spanish Research Agency* (MCI/AEI/FEDER, RTI218-096182-B-I00, CSIC13-4E-2076) and AGAUR (2017 SGR 208). G.S. L.R.-M. and J.-D.M. thank Spanish MINECO (grant CTQ2017-87889-P) and the *Generalitat de Catalunya* (2017SGR1323). G.S., thanks *Regione Autonoma della Sardegna* (grant RASSR79857) for his postdoctoral fellowship. L. R.-M. thanks the *Generalitat de Catalunya* for her FI fellowship. plasmid GFP-PCNAL2 was generously provided by Dr. Cristina Cardoso. Molecular graphics with *UCSF Chimera*, developed by the Resource for Biocomputing, Visualization, and Informatics at the University of California, San Francisco, with support from NIH P41-GM103311.[43] We are also grateful to Prof. Peter Scott of the IAS at the University of Warwick for his insights and advice during the preparation of this manuscript.

Keywords: DNA recognition • peptide design • metallopeptides • supramolecular chemistry • coordination chemistry

[1] a) W. M. Bloch, J. J. Holstein, B. Dittrich, W. Hiller, G. H. Clever, *Angew. Chem. Int. Ed.* **2018**, *57*, 5534–5538; b) J. J. Danon, A. Krüger, D. A. Leigh, J.-F. Lemonnier, A. J. Stephens, I. J. Vitorica-Yrezabal, S. L. Woltering, *Science* **2017**, *355*, 159–162; c) J.-F. Ayme, J. E. Beves, D. A. Leigh, R. T. McBurney, K. Rissanen, D. Schultz, *Nat. Chem.* **2012**, *4*, 15–20; d) J. P. Leonard, P. Jensen, T. McCabe, J. E. O'Brien, R. D. Peacock, P. E. Kruger, T. Gunnlaugsson, *J. Am. Chem. Soc.* **2007**, *129*, 10986-10987; e) B. S. Pilgrim, D. A. Roberts, T. G. Lohr, T. K. Ronson, J. R. Nitschke, *Nat. Chem.* **2017**, *9*, 1276–1281; f) Y. Inokuma, M. Kawano, M. Fujita, *Nat. Chem.* **2011**, *3*, 349–358.

[2] a) E. G. Baker, G. J. Bartlett, K. L. Porter Goff, D. N. Woolfson, *Acc. Chem. Res.* **2017**, *50*, 2085–2092; b) B. Dang, H. Wu, V. K. Mulligan, M. Mravic, Y. Wu, T. Lemmin, A. Ford, D.-A. Silva, D. Baker, W. F. DeGrado, *Proc. Natl. Acad. Sci. USA* **2017**, *114*, 10852–10857; c) H. Gradišar, S. Božič, T. Doles, D. Vengust, I. Hafner-Bratkovič, A. Mertelj, B. Webb, A. Šali, S. Klavžar, R. Jerala, *Nat. Chem. Biol.* **2013**, *9*, 362–366.

[3] a) E. Oheix, A. F. A. Peacock, *Chem. Eur. J.* **2014**, *20*, 2829–2839; b) Z. Zhou, G. Roelfes, *Nature Catalysis* **2020**, *3*, 289–294; c) S. M. Meier-Menches, A. Casini, *Bioconjug. Chem.* **2020**, *31*, 1279–1288; d) A. Jacques, C. Lebrun, A. Casini, I. Kieffer, O. Proux, J.-M. Latour, O. Sénèque, *Inorg. Chem.* **2015**, *54*, 4104–4113; e) H. Ishida, Y. Maruyama, M. Kyakuno, Y. Kodera, T. Maeda, S. Oishi, *ChemBioChem* **2006**, *7*, 1567–1570.

[4] a) C. Piguet, G. Bernardinelli, G. Hopfgartner, *Chem. Rev.* ***1997***, *97*, 2005-2062; b) M. Albrecht, *Chem. Rev.* ***2001***, *101*, 3457–3498; c) M. Albrecht, *Angew. Chem. Int. Ed.* **2005**, *44*, 6448–6451.

[5] a) J.-F. Ayme, J.-M. Lehn, C. Bailly, L. Karmazin, *J. Am. Chem. Soc.* **2020**, *142*, 5819–5824; b) J.-F. Ayme, J. E. Beves, C. J. Campbell, D. A. Leigh, *Angew. Chem. Int. Ed Engl.* **2014**, *53*, 7823–7827.

[6] D. E. Mitchell, G. Clarkson, D. J. Fox, R. A. Vipond, P. Scott, M. I. Gibson, *J. Am. Chem. Soc.* **2017**, *139*, 9835–9838.

[7] a) Y. Guan, Z. Du, N. Gao, Y. Cao, X. Wang, P. Scott, H. Song, J. Ren, X. Qu, *Sci Adv* **2018**, *4*, eaao6718; b) M. Li, S. E. Howson, K. Dong, N. Gao, J. Ren, P. Scott, X. Qu, *J. Am. Chem. Soc.* **2014**, *136*, 11655–11663.

[8] a) C. Zhao, H. Song, P. Scott, A. Zhao, H. Tateishi-Karimata, N. Sugimoto, J. Ren, X. Qu, *Angew. Chem. Int. Ed.* **2018**, *57*, 15723–15727; b) A. D. Faulkner, R. A. Kaner, Q. M. A. Abdallah, G. Clarkson, D. J. Fox, P. Gurnani, S. E. Howson, R. M. Phillips, D. I. Roper, D. H. Simpson, et al., *Nat. Chem.* **2014**, *6*, 797–803; c) R. A. Kaner, S. J. Allison, A. D. Faulkner, R. M. Phillips, D. I. Roper, S. L. Shepherd, D. H. Simpson, N. R. Waterfield, P. Scott, *Chem. Sci.* **2015**, *7*, 951–958; d) A. Oleksi, A. G. Blanco, R. Boer, I. Usón, J. Aymamí, A. Rodger, M. J. Hannon, M. Coll, *Angew. Chem. Int. Ed.* **2006**, *45*, 1227–1231; e) S. E. Howson, A. Bolhuis, V. Brabec, G. J. Clarkson, J. Malina, A. Rodger, P. Scott, *Nat. Chem.* **2012**, *4*, 31–36; f) X. Li, Z. Shi, J. Wu, J. Wu, C. He, X. Hao, C. Duan, *Chem. Commun.* **2020**, *56*, 7537–7548.

[9] a) G. Rama, A. Ardá, J.-D. Maréchal, I. Gamba, H. Ishida, J. Jiménez-Barbero, M. E. Vázquez, M. Vázquez López, *Chem. Eur. J.* **2012**, *18*, 7030–7035; b) I. Gamba, G. Rama, E. Ortega-Carrasco, R. Berardozzi, V. M. Sánchez-Pedregal, L. Di Bari, J.-D. Maréchal, M. E. Vázquez, M. Vázquez López, *Dalton Trans.* **2016**, *45*, 881–885.

[10] I. Gamba, G. Rama, E. Ortega-Carrasco, J.-D. Maréchal, J. Martínez-Costas, M. E. Vázquez, M. Vázquez López, *Chem. Commun.* **2014**, *50*, 11097–11100.

[11] a) S. R. Raghothama, S. K. Awasthi, P. Balaram, *J. Chem. Soc. Perkin Trans. 2* **1998**, 137–144; b) A. Fragoso, P. Lamosa, R. Delgado, O. Iranzo, *Chem. Eur. J.* **2013**, *19*, 2076–2088; c) M. D. Shults, B. Imperiali, *J. Am. Chem. Soc.* **2003**, *125*, 14248–14249.

[12] A. M. C. Marcelino, L. M. Gierasch, *Biopolymers* **2008**, *89*, 380–391.

[13] a) G. D. Rose, L. M. Glerasch, J. A. Smith, in Adv. Prot. Chem. (Eds.: C.B. Anfinsen, J.T. Edsall, F.M. Richards), Academic Press, 1985, pp. 1–109; b) V. Brenner, F. Piuzzi, I. Dimicoli, B. Tardivel, M. Mons, *Angew. Chem. Int. Ed.* **2007**, *46*, 2463–2466.

[14] M. G. Bomar, B. Song, P. Kibler, K. Kodukula, A. K. Galande, *Org. Lett.* **2011**, *13*, 5878–5881.

[15] a) J. DeRouchey, B. Hoover, D. C. Rau, *Biochemistry* **2013**, *52*, 3000–3009; b) S. M. West, R. Rohs, R. S. Mann, B. Honig, *J. Biomol. Struct. Dyn.* **2010**, *27*, 861–866; c) C. Crane-Robinson, A. I. Dragan, P. L. Privalov, *Trends Biochem. Sci.* **2006**, *31*, 547–552; d) D. P. Mascotti, T. M. Lohman, *Biochemistry* **1997**, *36*, 7272–7279.

[16] L. Cardo, V. Sadovnikova, S. Phongtongpasuk, N. J. Hodges, M. J. Hannon, *Chem. Commun.* **2011**, *47*, 6575–6577.

[17] I. Coin, M. Beyermann, M. Bienert, *Nat. Protoc.* **2007**, *2*, 3247–3256.

[18] We have omitted the charges to avoid confusion between the formal charges of the helicates and the actual charges of the complexes including the protonated Arg side chains and the N-terminal ammonium.

[19] To our surprise, while the 2,2'-bipyridine ligand is known to be weakly emissive, and for all practical purposes considered non-fluorescent, the 5'-amido-[2,2'-bipyridine]-5-carboxamide unit in the βAlaBpy building block was highly emissive (Φ ≈ 0.37). a) S. Dhanya, P. K. Bhattacharyya, *J. Photochem. Photobiol. A Chem.* **1992**, *63*, 179-185; b) M. Yagi, T. Kaneshima, Y. Wada, K. Takemura, Y. Yokoyama, *J. Photochem. Photobiol. A Chem.* **1994**, *84*, 27-32.

[20] a) P. Kuzmic, *Anal. Biochem.* **1996**, *237*, 260–273; P. Kuzmič, in *Methods Enzymol.*, Academic Press, **2009**, pp. 247–280.

[21] L. K. S. von Krbek, C. A. Schalley, P. Thordarson, *Chem. Soc. Rev.* **2017**, *46*, 2622–2637.

[22] J. M. Lehn, A. Rigault, J. Siegel, J. Harrowfield, B. Chevrier, D. Moras, *Proc. Natl. Acad. Sci. U. S. A.* **1987**, *84*, 2565–2569.

[23] W. M. Bloch, G. H. Clever, *Chem. Commun.* **2017**, *53*, 8506–8516.

[24] a) H. Crlikova, J. Malina, V. Novohradsky, H. Kostrhunova, R. A. S. Vasdev, J. D. Crowley, J. Kasparkova, V. Brabec, *Organometallics* **2020**, *39*, 1448–1455; b) M. J. Burke, G. S. Nichol, P. J. Lusby, *J. Am. Chem. Soc.* **2016**, *138*, 9308–9315; c) P. R. Symmers, M. J. Burke, D. P. August, P. I. T. Thomson, G. S. Nichol, M. R. Warren, C. J. Campbell, P. J. Lusby, *Chem. Sci.* **2015**, *6*, 756–760; d) D. A. Leigh, P. J. Lusby, R. T. McBurney, A. Morelli, A. M. Z. Slawin, A. R. Thomson, D. B. Walker, *J. Am. Chem. Soc*. **2009**, *131*, 3762–3771; e M. J. Burke, G. S. Nichol, P. J. Lusby, *J. Am. Chem. Soc.* **2016**, *138*, 9308–9315;) L. J. Charbonniere, G. Bernardinelli, C. Piguet, A. M. Sargeson, A. F. Williams, *J. Chem. Soc. Chem. Commun.* **1994**, 1419–1420.

[25] a) S. Auer, L. Azizi, F. Faschinger, V. Blazevic, T. Vesikari, H. J. Gruber, V. P. Hytönen, *Sens. Actuators B Chem.* **2017**, *243*, 104–113; b) S. V. Wegner, F. C. Schenk, J. P. Spatz, *Chem. Eur. J.* **2016**, *22*, 3156–3162; c) J. E. Hale, *Anal. Biochem.* **1995**, *231*, 46-49; d) S. V. Wegner, J. P. Spatz, *Angew. Chem. Int. Ed.* **2013**, *52*, 7593–7596

[26] Initial attempts at selective Co(II) to Co(III) oxidation using hydrogen peroxide were unsuccessful and resulted in complex product mixtures.

[27] S. D. Fairbanks, C. C. Robertson, F. R. Keene, J. A. Thomas, M. P. Williamson, *J. Am. Chem. Soc.* **2019**, *141*, 4644–4652

[28] K. Wüthrich, M. Billeter, W. Braun, *J. Mol. Biol*. **1984**, 715-740.

[29] S. Sreekantan Nair Lalithambika, R. Golnak, B. Winter, K. Atak, *Inorg. Chem.*, **2019**, *58*, 4731-4740.

[30] R. M. B. D.A. Case, W. Botello-Smith, D. S. Cerutti, T. E. Cheatham, III, T. A. Darden, R. E. Duke, T. J. Giese, H. Gohlke, A. W. Goetz, N. Homeyer, S. Izadi, P. Janowski, J. Kaus, A. Kovalenko, T. S. Lee, S. LeGrand, P. Li, C. Lin, T. Luchko, R. Luo, B. Madej, D. Mermelstein, K. M. Merz, G. Monard, H. Nguyen, H. T. Nguyen, I. Omelyan, A. Onufriev, D. R. Roe, A. Roitberg, C. Sagui, C. L. Simmerling, J. Swails, R. C. Walker, J. Wang, R. M. Wolf, X. Wu, L. Xiao, D. M. York, P. A. Kollman, AMBER 16, **2016**.

[31] Topological mirror images have previously been identified in proteins, but difficult to observe in small peptides, for which NMR data are often limited and lack well-defined secondary structure. a) J. K. Noel, A. Schug, A. Verma, W. Wenzel, A. E. Garcia, J. N. Onuchic, *J. Phys. Chem. B* **2012**, *116*, 6880–6888; b) K. A. Olszewski, A. Kolinski, J. Skolnick, *Proteins* **1996**, *25*, 286–299; c) A. Pastore, R. A. Atkinson, V. Saudek, R. J. Williams, *Proteins* **1991**, *10*, 22–32.

[32] a) J. Gómez-González, D. G. Peña, G. Barka, G. Sciortino, J.-D. Maréchal, M. Vázquez López, M. E. Vázquez, *Front Chem* **2018**, *6*, 520; b) C. R. K. Glasson, G. V. Meehan, J. K. Clegg, L. F. Lindoy, J. A. Smith, F. R. Keene, C. Motti, *Chem. Eur. J.* **2008**, *14*, 10535–10538.

[33] A similar effect has been reported recently in the binding of a self-assembled $Fe(II)_4L_4$ tetrahedron to a three-way junction DNA: J. Zhu, C. J. E. Haynes, M. Kieffer, J. L. Greenfield, R. D. Greenhalgh, J. R. Nitschke, U. F. Keyser, J. Am. Chem. Soc. **2019**, *141*, 11358–11362, and is consistent with energy transfer through the DNA bases between the fluorophores: a) K. Börjesson, S. Preus, A. H. El-Sagheer, T. Brown, B. Albinsson, L. M. Wilhelmsson, *J. Am. Chem. Soc.* **2009**, *131*, 4288–4293; b) A. Kuhlmann, L. Bihr, H.-A. Wagenknecht, *Angew. Chem. Int. Ed Engl.* **2020**, 59, 17378–17382.

[34] a) L. M. Hellman, M. G. Fried, *Nature Protocols* **2007**, *2*, 1849–1861; b) D. Lane, P. Prentki, M. Chandler, *Microbiol. Rev.* **1992**, *56*, 509–528; c) R. S. Tuma, M. P. Beaudet, X. Jin, L. J. Jones, C. Y. Cheung, S. Yue, V. L. Singer, *Anal. Biochem.* **1999**, *268*, 278–288.

[35] The smearing and disappearance of bands at high concentrations has been attributed to the existence of multiple binding complexes and the precipitation of the DNA conjugates, see for example: a) E. K. Liebler, U. Diederichsen, *Org. Lett.* **2004**, *6*, 2893–2896; b) O. Vázquez, M. E. Vázquez, J. B. Blanco, L. Castedo, J. L. Mascareñas, *Angew. Chem. Int. Ed*. **2007**, *46*, 6886–6890; c) G.-X. He, K. A. Browne, A. Blasko, T. C. Bruice, J. Am. Chem. Soc. 1994, 116, 3716–3725; d) C. Portela, F. Albericio, R. Eritja, L. Castedo, J. L. Mascareñas, *ChemBioChem* **2007**, *8*, 1110–1114.

[36] GaudiMM is a molecular builder designed to produce physically sound models of complex systems by exploring the conformational space that satisfies a series of molecular descriptors and adapted to perform flexible molecular docking exploring large dimensional spaces: J. Rodríguez-Guerra Pedregal, G. Sciortino, J. Guasp, M. Municoy and J.-D. Maréchal, *J. Comput. Chem.*, **2017**, *38*, 2118–2126.

[37] Prepared *in situ* by mixing a 5 μM **TAMRA-LLD** or Flu-**LLD** peptide ligand with 25 μM $(NH_4)_2Fe(SO_4)_2$.

[38] We observed a drastic effect of the fluorophore in the internalization, so that the fluorescein-tagged helicate remains adsorbed to the plasma membrane, while the rhodamine derivative is internalized. Similar effects have been previously observed with metal complexes: C. A. Puckett, J. K. Barton, *J. Am. Chem. Soc.* **2009**, *131*, 8738–8739.

[39] Digitonin is a widely used additive used to transiently permeabilize the plasma membrane: a) M. Nishikawa, S. Nojima, T. Akiyama, U. Sankawa, K. Inoue, *J. Biochem*. **1984**, *96*, 1231–1239; b) M. P. Stewart, R. Langer K. F. Jensen, *Chem. Rev*. **2018**, *118*, 7409–7531.

[40] a) H. Leonhardt, H. P. Rahn, P. Weinzierl, A. Sporbert, T. Cremer, D. Zink, M. C. Cardoso, *J. Cell Biol*. **2000**, *149*, 271–280; b) R. Yokoyama, T. Hirakawa, S. Hayashi, T. Sakamoto, S. Matsunaga, *Sci. Rep.* **2016**, *6*, 29657.

[41] L. S. Shlyakhtenko, V. N. Potaman, R. R. Sinden, A. A. Gall, Y. L. Lyubchenko, *Nucleic Acids Res.* **2000**, *28*, 3472–3477.

[42] Phongtongpasuk, S. Paulus, J. Schnabl, R. K. O. Sigel, B. Spingler, M. J. Hannon, E. Freisinger, *Angew. Chem. Int. Ed*. ***2013***, *52*, 11513–11516.

[43] E. F. Pettersen, T. D. Goddard, C. C. Huang, G. S. Couch, D. M. Greenblatt, E. C. Meng, T. E. Ferrin, *J. Comput. Chem.* **2004**, *25*, 1605–1612.

10.1002/anie.202013039

WILEY-VCH

RESEARCH ARTICLE

Entry for the Table of Contents

COMMUNICATION

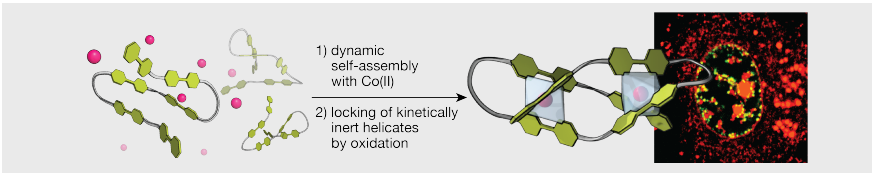

Artificial bipyridine-containing peptide ligands encode in their sequence the stereoselective folding into chiral three-stranded Fe(II) or Co(II) peptide helicates, and as kinetically-inert dinuclear Co(III) complexes by in situ oxidation. These peptide helicates selectively label DNA replication foci in functional cells.

J. Gómez-González, Y. Pérez, G. Sciortino, L. Roldán-Martín, J. Martínez-Costas, J.-D. Maréchal, I. Alfonso, M. Vázquez López, M. E. Vázquez**

Page No. – Page No.

Dynamic Stereoselection of Peptide Helicates and Their Selective Labeling of DNA Replication Foci in Cells